

On Bias and Its Reduction via Standardization in Source Localization Problems

Joonas Lahtinen

Mathematics & Computing Sciences, Tampere University, Tampere 33720, Finland

E-mail: `joonas.j.lahtinen@tuni.fi`

Abstract. In source localization problems, the aim is to locate the sources within a domain that causes given measurements on the boundary. In this type of problem, biasing of the solution is one of the main causes of mislocalization. A technique called standardization was developed to reduce biasing. However, the lack of a mathematical background for this method can cause difficulties in its application and confusion regarding the reliability of solutions. Here, we give a rigorous and generalized background for the technique using the Bayesian framework to shed light on the technique's abilities and limitations. In addition, we take a look at the noise robustness of the method that is widely reported in numerical studies. The paper starts by giving a gentle introduction to the problem and its bias and works its way toward standardization.

Keywords: Linear forward problem, Point source reconstruction, Source localization, Solution bias

Submitted to: *Inverse Problems* 07-Mar-2024

1. Introduction

The inverse source localization problem of the Poisson equation takes the following form under Neumann boundary conditions:

$$\nabla \cdot (M \nabla u) = f \quad \text{in } \Omega, \quad (1)$$

$$\mathbf{n} \cdot (M \nabla u) = g \quad \text{on } \partial\Omega, \quad (2)$$

for any $f \in L^2(\Omega)$ and $g \in L^2(\partial\Omega)$, where tensor-valued M encodes the conductivity of the domain and \mathbf{n} denotes an outward unit normal vector of Ω . The goal is to localize the few small pointwise compact supports of the source term. Such a problem can arise, e.g., in the electromagnetic inverse source problem [1, 2], electrocardiography inverse problem [3], and inverse problems of geophysics [4] such as electrical resistance tomography [5, 6]. In these cases, among many others, the problem is linearised to obtain the numerical solution due to the domain being geometrically complex and inhomogeneous by its parameters. For example, in the quasi-static electromagnetic inverse source localization problem [7], the usage of a realistic model of the head and folded brain structure helps to locate the brain activity [8, 9], geometrically detailed model also helps estimate cardiac electrical activity from voltage distributions measured on the body surface in electrocardiography inverse problem [10]. Moreover, in this ill-conditioned problem, the measurements obtained from the domain's boundary are considered noisy. Thus, one need to solve such a $\mathbf{x} \in \mathbb{R}^n$ from the linear inverse problem

$$\mathbf{y} = L\mathbf{x} + \mathbf{q}, \quad (3)$$

that it has a set of non-zero values within the support of f . Here the $\mathbf{y} \in \mathbb{R}^m$ denotes measurements, $L \in \mathbb{R}^{m \times n}$ is the system matrix, and noise vector $\mathbf{q} \in \mathbb{R}^m$ is assumed to follow zero-mean Gaussian distribution $\mathcal{N}(\mathbf{0}, C)$ with measurement noise covariance matrix $C \in \mathbb{R}^{m \times m}$.

The support of f is often assumed to be compounded from a few distinct points called *true sources*. One possible approach is to use a sparse solver to reconstruct a nearly point-like source. However, more complex algorithms pose limitations to the forward model's resolution, thus making a trade-off between spatial accuracy and the sparsity of the solution, e.g., in the case of the well-known LASSO when it is implemented using Least Angle Regression algorithm [11]. Consequently, the practice has been to use lighter inverse algorithms and choose the component of the reconstructed parameter vector with the largest magnitude as the indicator of source location [12, 13, 14]. This localization practice has been demonstrated to be robust and reliable with a range of inversion methods [15, 16].

As the forward modeling incorporates with probabilistic interpretation of the noise, Bayesian modeling can be considered appropriate for regularization [17]. Consider a common Gaussian process regression model, also called Bayesian minimum norm estimate (BMNE) [18], with a posterior composed of a Gaussian likelihood $\mathbf{y} \mid \mathbf{x} \sim \mathcal{N}(L\mathbf{x}, C)$ and a Gaussian prior $\mathbf{x} \sim \mathcal{N}(\mathbf{0}, \Gamma)$, where $\Gamma \in \mathbb{R}^{n \times n}$ is a diagonal prior covariance. An estimate for the realization of \mathbf{x} can be obtained as the *maximum a*

posteriori (MAP)

$$\hat{\mathbf{x}} = \arg \max_{\mathbf{x} \in \mathbb{R}^n} \{ \mathcal{N}(L\mathbf{x}, C) \times \mathcal{N}(\mathbf{0}, \Gamma) \}, \quad (4)$$

which constitutes the following $L2$ – $L2$ minimization problem, whose objective function is composed of a $L2$ norm-based data fit and regularization term the latter one of which can be associated with Tikhonov regularization:

$$\min_{\mathbf{x} \in \mathbb{R}^n} \{ (\mathbf{y} - L\mathbf{x})^T C^{-1} (\mathbf{y} - L\mathbf{x}) + \mathbf{x}^T \Gamma^{-1} \mathbf{x} \}. \quad (5)$$

This model, however, poses some challenges: Due to the maximum principle of elliptic partial differential equations [19, 20], the maximum of the forward problem lies on the boundary. Consequently, it biases the estimated source locations to the part of the boundary where the measurement sensors are located. The most intuitive approach to tackle bias is to use solution weighting that utilizes some norm of the system matrix columns [21, 22]. This, however, could reduce the bias only depth-wise away from the measurement sensors. More comprehensive unbiasing can be achieved by weighting the regularization so that the point spread of each covered parameter is taken into account [23, 24] in which case complete unbiasing can be achieved with noiseless data and when the regularization parameter tends to zero. As the third known way to counter the bias, Pascual-Marqui has introduced the technique called *standardization* [14], where the components of an inverse solution are post-hoc weighted by the square roots of the diagonal elements of the resolution matrix, that is

$$R = \Gamma L^T (L \Gamma L^T + C)^{-1} L \quad (6)$$

as derived in [25], to form unbiased estimations for covering the location of a single source. Resolution matrix is also known as Backus-Gilbert resolution kernel [26, 27]. It defines a relation between inverse solution and forward model parameters under linear inversion, essentially in $L2$ – $L2$ minimization. It is mainly applied to electromagnetic source imaging [28] and inversion problems of geophysics [25]. The matrix can be used to estimate the resolution length of the estimation when the forward and inverse models are known, and its diagonal elements are interpreted to evaluate the resolvability of the target source [29]. Here we define localization bias as in [13] saying that the solution is unbiased when the point-spread function has its maximum at the correct source location, this means that the k th resolution matrix column has its maximum component at k th entry, as we will see later. This definition assumes no uncertainty related to the forward model.

Due to the formulation of the weights, the standardization weighting procedure is closely related to the standardization of Gaussian random variables as the marginal distribution of MAP for k th entry is $\mathcal{N}(\mathbf{0}, R_{kk})$. The localization of the source via standardization of Gaussian process regression has been previously shown to be simultaneously unbiased and errorless under specific conditions [30, 31], e.g., using the boundary of a volumetric structure as the domain for calculations. By errorless, we mean that the entry with the maximum magnitude of MAP estimate corresponds to the

location of the true source. Moreover, the robustness of the method to the measurement noise was described in [32, 33].

Even though standardization has been successfully applied in brain imaging [34, 35, 36], its theoretical foundation remains unexplored and thus it is yet unclear when this method performs well and what are the conditions under which we can recover an exact source location. This work aims to shed light on the theoretical background of the standardization and to provide the theoretical framework to apply standardization to problems that are modeled with the help of the Poisson differential equation. In particular, we consider the standardization technique within a general discretized Poisson-type forward problem and a general Gaussian process regression model for inversion to answer these open questions. In practice, we analyze the forward model-induced localization bias related to the L_2 -norm data fitting and how standardization can reduce it through simple settings. In this study, we are working under the assumption that there is only one source to be localized and the discretized forward model describes reality reasonably well, i.e., there is no uncertainty related to it. In our analysis, it means that measurement can be written as $\mathbf{y} = a\mathbf{L}_k$, where \mathbf{L}_k is k th column of the system matrix and a is source strength. As we will see later, we can bypass the limitation of one source by generalizing the standardization technique for every zero-mean Gaussian prior and using an educated guess about the prior via Kalman filtering.

As our main contributions, we formalize a Bayesian extension of the technique itself, derive the general conditions for perfect localization via the maximum of the reconstruction, and examine the noise robustness of the localization by deriving a lower bound probability for perfect localization for Gaussian distributed measurements. In numerical examples, we demonstrate how multiple simultaneous and correlated sources can be recovered and tracked via the generalized formulation of standardization which is an impossible task with the original standardization [37, 38], and we demonstrate how the lower bound relates to the observed localization results.

The paper is structured as follows. The forward problem and standardized inversion method will be introduced in Section 2. The forward model-induced localization bias and how standardization reduces it is examined in Section 3. The necessary conditions for perfect localization via standardization are presented in Section 4. The lower probability limit for perfect localization from Gaussian distributed data is presented in Section 5. Computational examples of unbiased localization and noise durability are given in Section 6. Finally, this paper ends with a discussion and conclusion.

2. Methods

2.1. Standardized low-resolution brain tomography as probabilistic model

In this section, we give a probabilistic interpretation of the standardization technique introduced in [14]. Simultaneously, we generalize the original underlying prior model

one step further assuming independent but not identically Gaussian distributed sources. Standardization is a post-hoc weighting of minimum norm estimate [18] developed to overcome its localization bias. Namely, the method aims to have the highest magnitude of the reconstruction to be located where the true source lies, and thus it produces unbiased estimations in noiseless situations when considering that there are no modeling uncertainties, i.e., models are perfect.

Let us assume that there is a random source spread and placement $\underline{\mathbf{x}} \sim \mathcal{N}(\mathbf{0}, \Gamma)$ and noise vector $\underline{\mathbf{n}} \sim \mathcal{N}(\mathbf{0}, C)$ forming the randomized measurements $\underline{\mathbf{y}} = L\underline{\mathbf{x}} + \underline{\mathbf{n}}$. The task is to find the most probable originator for the source spread. This corresponds to the minimization problem of the form (5) in which L has been substituted with $L\Gamma^{1/2}$ as the forward operator, where $[\Gamma^{1/2}]_{ii} = \Gamma_{ii}^{1/2}$, and identity matrix as the Tikhonov regularization matrix. Because of this, we are able to rewrite the measurements as $\underline{\mathbf{y}} = L\Gamma^{1/2}\underline{\mathbf{u}} + \underline{\mathbf{n}}$ where naturally $\underline{\mathbf{u}} \sim \mathcal{N}(\mathbf{0}, I)$.

A rigorous definition for the post-hoc weights can be given by filling in the blanks via probability theory from the reasoning in [14]: Since the resolution matrix itself is an intermodel concept, we should also consider the weighted reconstruction as such, and therefore, we could derive the distribution of measurements via marginalized likelihood, i.e.,

$$\pi(\underline{\mathbf{y}}) = \int_{\Omega} \mathcal{N}(L\Gamma^{1/2}\underline{\mathbf{u}} \mid C) \mathcal{N}(\underline{\mathbf{u}} \mid I) d\underline{\mathbf{u}} = \mathcal{N}(\mathbf{0} \mid L\Gamma L^T + C) \quad (7)$$

from which one could define the distribution for MAP estimator of $\underline{\mathbf{u}}$ as

$$\pi(\hat{\underline{\mathbf{u}}}) = \pi(\Gamma^{-1/2}L^\dagger \underline{\mathbf{y}}) = \mathcal{N}(\mathbf{0}, \Gamma^{-1/2}R\Gamma^{1/2}). \quad (8)$$

In addition, one should remark that $\hat{\underline{\mathbf{u}}}$ is not a MAP estimator of the original source localization problem. It is then required to project the standardized estimation back via $\Gamma^{1/2}$. Consequently, by component-wise standardizing $\hat{\underline{\mathbf{u}}}$ for some sampled $\underline{\mathbf{y}}$, we obtain

$$\mathbf{e}_k^T \Gamma^{-1/2} \mathbf{z} = \frac{\mathbf{e}_k^T \Gamma^{-1/2} L^\dagger \underline{\mathbf{y}}}{\sqrt{\mathbf{e}_k^T \Gamma^{-1/2} R \Gamma^{1/2} \mathbf{e}_k}}, \quad (9)$$

where \mathbf{e}_k is k th unit basis vector of \mathbb{R}^n and $\mathbf{z} \in \mathbb{R}^n$ is the parameter vector corresponding to the original source localization problem. Since Γ is diagonal,

$$z_k = \frac{\mathbf{e}_k^T \Gamma L^T (L\Gamma L^T + C)^{-1} \underline{\mathbf{y}}}{\sqrt{\mathbf{e}_k^T R \mathbf{e}_k}} = R_{kk}^{-1/2} \hat{x}_k \quad (10)$$

of which the largest in absolute value is chosen to indicate the estimated position of the source.

The standardization technique is analogical to the Gaussian standardization of the previous MAP estimation applied to each vector component individually. It means that each projection $[L\Gamma^{1/2}]_k$ to measurement space is as many standard deviations away from the mean that is zero. This is equivalent to Z-scores [37, 39], where a set of Gaussian random variables from different scales are unified to ensure a fair comparison.

As standardization is a weighting of the solution vector depending only on the model parameters, we are able to write the standardized minimum problem as the following

minimization problem

$$\min_{\mathbf{z} \in \mathbb{R}^n} \{ (\mathbf{y} - L\mathbf{T}\mathbf{z})^T C^{-1} (\mathbf{y} - L\mathbf{T}\mathbf{z}) + \mathbf{z}^T T^T \Gamma^{-1} T \mathbf{z} \}, \quad (11)$$

where $T = \text{Diag}(R)^{1/2}$ and $\text{Diag}(R)$ denotes a diagonal matrix with $\text{diag}(R)$ as its diagonal elements. It should be noted that due to the formulation of the standardization, the technique works best in locating one source. The shortcomings of the method in locating several simultaneous sources have been demonstrated before [38].

3. Localization bias of BMNE and its reduction

In this section, we examine which model parameters are responsible for the solution bias of BMNE, i.e., which one determines the component of the reconstruction vector with the largest absolute value. For that reason, we need to consider the orthogonal decomposition of system matrix columns to parallel with measurement \mathbf{y} and components normal to it. We could see these components of decomposition as how much a column \mathbf{L}_k of the system matrix contributes to explaining the measurements and how much of it is a nuisance. To measure the proportion that a vector is parallel to measurement, we use normalized scalar projection (NSP)

$$\text{proj}_{\mathbf{y}}(\mathbf{L}_k | C) = \frac{\mathbf{y}^T C^{-1} \mathbf{L}_k}{\sqrt{\mathbf{y}^T C^{-1} \mathbf{y} \mathbf{L}_k^T C^{-1} \mathbf{L}_k}} \quad (12)$$

presented for k th system matrix column, from which we can define normalized scalar rejection as $1 - \text{proj}_{\mathbf{y}}(\mathbf{L}_k | C)$. Utilizing the latter one, we can obtain that orthogonal sets exist, for example, in a homogenous conductivity disk in Figure 1. From the illustration, we see how the perpendicular set is larger for a source far from the sensors, indicating that the accurate localization of such a source is more difficult than a source near sensors.

3.1. Example: localization bias of Minimum norm estimate in three source locations

Let us find the reconstruction $\hat{\mathbf{x}} = [\hat{x}_1, \hat{x}_2, \hat{x}_3]$ of a point source. As an illustration, assume that the system matrix can be written as $L = [\mathbf{L}_1, a\mathbf{L}_1, \mathbf{L}_3]$, where $a \in \mathbb{R}$. Now, assuming that we have a perfect forward model and the true source is at the location of component 1, meaning that \mathbf{y} is parallel with \mathbf{L}_1 . To simplify the notation, we define $\mathbf{y} = \mathbf{L}_1$, and Mahalanobis distance as

$$\rho(\mathbf{u}, \mathbf{v} | \Sigma) = \sqrt{(\mathbf{u} - \mathbf{v})^T \Sigma^{-1} (\mathbf{u} - \mathbf{v})}. \quad (13)$$

By utilizing Mahalanobis distance, we can decompose another system matrix entry \mathbf{L}_3 in parallel and orthogonal part with respect to \mathbf{L}_1 such that

$$\rho(\mathbf{L}_3, \mathbf{0} | C)^2 = \rho(b\mathbf{L}_1, \mathbf{0} | C)^2 + \rho(\mathbf{L}_1^\perp, \mathbf{0} | C)^2 \quad (14)$$

for some $b \in \mathbb{R}$. Within this notation, the minimization problem (5) can be written as

$$\min_{\mathbf{x} \in \mathbb{R}^3} \{ \rho(\mathbf{L}_1, \mathbf{L}_1 x_1 + a\mathbf{L}_1 x_2 + b\mathbf{L}_1 x_3 | C)^2 + \rho(\mathbf{0}, \mathbf{L}_1^\perp x_3 | C)^2 + \rho(\mathbf{0}, \mathbf{x} | \Gamma)^2 \}. \quad (15)$$

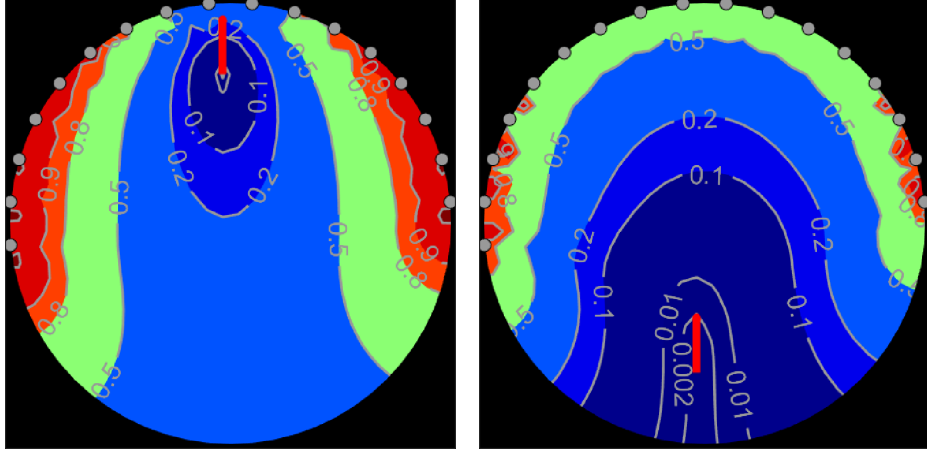


Figure 1. Here we plot the normalized scalar rejection $1 - \text{proj}_{\mathbf{y}}(\mathbf{L}_k \mid I)$ for two different source configurations. A homogeneous conductivity disk where measurement sensors are on the upper half of the disk (grey balls) is used as the modeling scheme. Low values (dark blue area) are achieved when the columns of the system matrix associated with this area are almost or completely parallel (as vectors) to measurements caused by the source indicated via the red arrow. Values near 1 are achieved when the columns are normal to measurement. The exact value 1 is indicated via dark red coloring. Decomposing each column of the system matrix to a vector that can explain the measurements (that is parallel in the optimal case) and nuisance part (normal) helps us to understand the depth bias obtained from the estimator. The left image shows the value contours for a source near sensors, and the right-hand-side one represents a situation where the source is far from the sensors.

Moreover, when the 3×3 prior covariance is diagonal,

$$\Gamma = \begin{bmatrix} p_1 & 0 & 0 \\ 0 & p_2 & 0 \\ 0 & 0 & q \end{bmatrix}, \quad (16)$$

the solution is of the form

$$\begin{bmatrix} \hat{x}_1 \\ \hat{x}_2 \\ \hat{x}_3 \end{bmatrix} = \begin{bmatrix} p_1 \mathbf{L}_1^T (L^T \Gamma L + C)^{-1} \mathbf{L}_1 \\ a p_2 \mathbf{L}_1^T (L^T \Gamma L + C)^{-1} \mathbf{L}_1 \\ b(q^{-1} + (\mathbf{L}_1^\perp)^T C^{-1} \mathbf{L}_1^\perp)^{-1} \mathbf{L}_1^T (L^T \Gamma L + C)^{-1} \mathbf{L}_1 \end{bmatrix} \quad (17)$$

We can easily see that the localization estimation is correct, i.e., absolute value \hat{x}_1 is the largest if and only if

$$p_1 > |a| p_2 \quad \text{and} \quad p_1 > |b| (q^{-1} + (\mathbf{L}_1^\perp)^T C^{-1} \mathbf{L}_1^\perp)^{-1}. \quad (18)$$

Relations between the expressions p_1 , $|a| p_2$, and $|b| (q^{-1} + (\mathbf{L}_1^\perp)^T C^{-1} \mathbf{L}_1^\perp)^{-1}$ in the inequalities dictate the biasing of the inverse solution. In effect, the system matrix columns model the measurements produced by sources in different locations. Due to the maximum principle, the columns corresponding to sources near the boundary will have higher absolute values than a column corresponding to a deeper interior location. If the estimated variables are assumed to be identically distributed, meaning that there is a positive number δ that $\Gamma = \delta I$, then the location of the maximum entry of the

reconstruction mostly depends on the system matrix values if the system matrix columns are not distinct enough, i.e., NSP is high between columns of the system matrix.

3.2. Standardization reduces solution bias

In this section, we show that the standardization technique introduced in 2.1 reduces the bias of BMNE presented in the previous section. In practice, we show that the set of parameter vector components attaining the maximum magnitude is analogical with the set of individual system matrix columns that are parallel with given measurements \mathbf{y} . Here we denote the subset of system matrix column indices that are parallel to measurement \mathbf{y} by

$$\mathcal{S}(\mathbf{y}) = \{k \in [1, n] : \text{proj}_{\mathbf{y}}(\mathbf{L}_k \mid C) = 1\}. \quad (19)$$

In this example, it means that there exists a real number s_k for such that $\mathbf{L}_k = s_k \mathbf{y}$, when $k \in \mathcal{S}(\mathbf{y})$. Standardization weights are defined as the reciprocal of the square root of diagonal elements of the resolution matrix

$$R_{kk} = \Gamma_{kk} \mathbf{L}_k^T (L\Gamma L^T + C)^{-1} \mathbf{L}_k. \quad (20)$$

If we now assume that the measurement data is produced by a unit-strength source at location i , i.e., $\mathbf{y} = \mathbf{L}_i$, we obtain that every standardized component corresponding to the set $\mathcal{S}(\mathbf{y})$ have the form

$$|z_k| = \left| \frac{s_k \Gamma_{kk} \mathbf{L}_i^T (L\Gamma L^T + C)^{-1} \mathbf{L}_i}{\sqrt{s_k^2 \Gamma_{kk} \mathbf{L}_i^T (L\Gamma L^T + C)^{-1} \mathbf{L}_i}} \right| = \sqrt{\Gamma_{kk} \mathbf{L}_i^T (L\Gamma L^T + C)^{-1} \mathbf{L}_i}, \quad (21)$$

meaning that the component values are only distinguished by the values of the diagonal prior but not by the magnitude of the corresponding system matrix's elements. Moreover, the standardized reconstruction has its maximum component at every index $k \in \mathcal{S}(\mathbf{y})$ as shown next.

Lemma 3.1. *Supremum of*

$$\sup_{\mathbf{u} \in \mathbb{R}^n} \left| \frac{\mathbf{u}^T \Sigma^{-1} \mathbf{v}}{(\mathbf{u}^T \Sigma^{-1} \mathbf{u})^{1/2}} \right| \quad (22)$$

is obtained for \mathbf{u} parallel with \mathbf{v} , where \mathbf{v} is non-zero vector and Σ is positive definite.

Proof. We can see by straight calculation that

$$\sup_{\mathbf{u}} \left| \frac{\mathbf{u}^T \Sigma^{-1} \mathbf{v}}{(\mathbf{u}^T \Sigma^{-1} \mathbf{u})^{1/2}} \right| = \sup_{\hat{\mathbf{u}}} \left| \frac{\hat{\mathbf{u}}^T \hat{\mathbf{v}}}{(\hat{\mathbf{u}}^T \hat{\mathbf{u}})^{1/2}} \right| = \|\hat{\mathbf{v}}\|_2 = (\mathbf{v}^T \Sigma^{-1} \mathbf{v})^{1/2}, \quad (23)$$

due to the positive definiteness of the matrix Σ , and the supremum is reached with \mathbf{u} parallel with \mathbf{v} . \square

It follows that in our case of the Bayesian model, the maximum reconstruction vector component is the one having maximum prior variance Γ_{kk} , where $k \in \mathcal{S}(\mathbf{y})$. Therefore, the prior model can be used to guide the solution to a certain region based on the prior information on the source location and to avoid the possible case where the

solution is non-unique due to $\mathcal{S}(\mathbf{y})$ containing more than one index. The alternative unbiasing technique called *exact low-resolution electromagnetic tomography* (eLORETA) [23] is less flexible in this regard because the weighted regularization is fixed, and thereby, does not allow any alternation of the solution via prior information.

Moreover, we can connect standardization with Mahalanobis distance by noticing

$$\sqrt{\Gamma_{jj}\mathbf{L}_j^T(L\Gamma L^T + C)^{-1}\mathbf{L}_j} = \sqrt{\Gamma_{jj}}\rho(\mathbf{0}, \mathbf{L}_j \mid L\Gamma L^T + C), \quad (24)$$

where the distance is taken with respect to the distribution of measurements as a marginal distribution from the likelihood. Standardization by this Mahalanobis distance can be interpreted so that each projection \mathbf{L}_j from the source space to the measurement space is equally achievable by the distribution of measurements, i.e., they are as many standard deviations away from the mean.

4. Generalized case: Gaussian distributed source configuration

To expand the theory presented in Section 2.1, we consider general prior covariance instead of diagonal ones. For that reason, we use the matrix square roots, calculated utilizing Schur factorization [40], in the modified system matrix $L\Gamma^{1/2}$. One could use the left Cholesky factor of Γ instead, but we make our decision for the sake of simplicity in notations and this particular decomposition is suggested to be used [30] due to its symmetry. In this section, we show that we have a similar index set for maximizing components for reformulated problems as the one presented in the previous section. Likewise in Section 2.1, we consider randomized measurements written as $\underline{\mathbf{y}} = L\Gamma^{1/2}\underline{\mathbf{u}} + \underline{\mathbf{n}}$. We introduce notation $\hat{L} = L\Gamma^{1/2}$ to simplify the writings.

Let us define the decomposition of the new system matrix first, denoting

$$\hat{K} = [L\Gamma^{1/2}]_k, \quad k \in \hat{\mathcal{S}}(\mathbf{y}), \quad (25)$$

where

$$\hat{\mathcal{S}}(\mathbf{y}) = \{k \in [1, n] : \text{proj}_{\mathbf{y}}([L\Gamma^{1/2}]_k \mid C) = 1\}, \quad (26)$$

and

$$\hat{H} = [L\Gamma^{1/2}]_k, \quad k \in [1, n] \setminus \hat{\mathcal{S}}(\mathbf{y}). \quad (27)$$

The following theorem states that the index set $\hat{\mathcal{S}}(\mathbf{y})$ is, in fact, the set of nodes having maximum reconstruction value for this newly formatted problem.

Theorem 4.1. *For a standardized minimum norm problem*

$$\min_{\mathbf{z} \in \mathbb{R}^n} \left\{ \rho(\mathbf{y}, \hat{K}\hat{T}\mathbf{z} + \hat{H}\hat{T}\mathbf{z} \mid C)^2 + \rho(\mathbf{0}, \hat{T}\mathbf{z} \mid I)^2 \right\}, \quad (28)$$

where

$$\hat{T} = \text{Diag} \left(\begin{bmatrix} \hat{K}^T \\ \hat{H}^T \end{bmatrix} \left(\begin{bmatrix} \hat{K} & \hat{H} \end{bmatrix} \begin{bmatrix} \hat{K}^T \\ \hat{H}^T \end{bmatrix} + C \right)^{-1} \begin{bmatrix} \hat{K} & \hat{H} \end{bmatrix} \right)^{1/2}, \quad (29)$$

if there exists a particular solution \mathbf{v}_0 for $\hat{K}\mathbf{v}_0 = \mathbf{y}$, where the sub-system matrix is given by Equation 25, the maximum components of the reconstruction vector \mathbf{z} corresponds the system matrix column that can be written as $\hat{K}\mathbf{v}$ and \mathbf{v} belongs to the vector space $\text{span}(\mathbf{v}_0)$.

Proof. The problem of finding the maximizing index

$$\arg \max_{i \in [1, n]} \left\{ \frac{\mathbf{A}_i^T \Sigma^{-1} \mathbf{y}}{\sqrt{\mathbf{A}_i^T \Sigma^{-1} \mathbf{A}_i}} \right\}, \quad (30)$$

where \mathbf{A}_i is the i th column vector of the matrix $A = [\hat{K} \ \hat{H}]$ and $\Sigma = AA^T + C$, can be written as the following maximization problem

$$\text{maximize } \mathbf{x}^T A^T \Sigma^{-1} \mathbf{y} \quad \text{subject to } \sqrt{\mathbf{x}^T A^T \Sigma^{-1} A \mathbf{x}} = c, \quad (31)$$

for some $c > 0$. The problem can be solved by first forming the following Lagrangian

$$\mathcal{L}(\mathbf{x}, \lambda) = \mathbf{x}^T A^T \Sigma^{-1} \mathbf{y} - \lambda(\sqrt{\mathbf{x}^T A^T \Sigma^{-1} A \mathbf{x}} - c) \quad (32)$$

and then calculating the derivatives

$$\frac{\partial \mathcal{L}}{\partial \mathbf{x}} = (A^T \Sigma^{-1} \mathbf{y})^T - \frac{\lambda \mathbf{x}^T A^T \Sigma^{-1} A}{\sqrt{\mathbf{x}^T A^T \Sigma^{-1} A \mathbf{x}}}, \quad (33)$$

$$\frac{\partial \mathcal{L}}{\partial \lambda} = c - \sqrt{\mathbf{x}^T A^T \Sigma^{-1} A \mathbf{x}}. \quad (34)$$

By setting these to zero, we get

$$A^T \Sigma^{-1} \left(\mathbf{y} - \frac{\lambda}{c} A \mathbf{x} \right) = \mathbf{0}. \quad (35)$$

Unless $\Sigma^{-1}(\mathbf{y} - (\lambda/c)\mathbf{A}_k)$ belong to the null-space of A^T for some $k \in [1, n] \setminus \hat{\mathcal{S}}(\mathbf{y})$ and $\lambda \in \mathbb{R}$ which cannot be realized since \mathbf{y} is assumedly image of A , therefore, there are no local maxima for that index set. Contrarily there exists maximizing index $k \in \hat{\mathcal{S}}(\mathbf{y})$ by definition.

In addition, we can write a new maximization problem for the second case, noting that optimum should contain a vector linearly dependent on \mathbf{y} , and also $\mathbf{y}^T \Sigma^{-1} \mathbf{y}$ does not affect on maximum so that it can be neglected from the problem statement, that is

$$\text{maximize } \mathbf{x}^T \hat{H}^T \Sigma^{-1} \mathbf{y} \quad \text{subject to } \sqrt{(\hat{H} \mathbf{x} + \mathbf{y})^T \Sigma^{-1} (\hat{H} \mathbf{x} + \mathbf{y})} = c. \quad (36)$$

Solving this similarly as above, derivatives of this Lagrangian are

$$\frac{\partial \mathcal{L}}{\partial \mathbf{x}} = (\hat{H}^T \Sigma^{-1} \mathbf{y})^T - \lambda \frac{\mathbf{x}^T \hat{H}^T \Sigma^{-1} \hat{H} + \mathbf{y}^T \Sigma^{-1} \hat{H}}{\sqrt{(\hat{H} \mathbf{x} + \mathbf{y})^T \Sigma^{-1} (\hat{H} \mathbf{x} + \mathbf{y})}}, \quad (37)$$

$$\frac{\partial \mathcal{L}}{\partial \lambda} = c - \sqrt{(\hat{H} \mathbf{x} + \mathbf{y})^T \Sigma^{-1} (\hat{H} \mathbf{x} + \mathbf{y})}. \quad (38)$$

Yielding to the equation

$$\hat{H}^T \Sigma^{-1} \left(\left(1 - \frac{\lambda}{c} \right) \mathbf{y} - \frac{\lambda}{c} \hat{H} \mathbf{x} \right) = \mathbf{0} \quad (39)$$

that has the solution $(\mathbf{x}, \lambda) = (\text{null}(\hat{H}^T \Sigma^{-1} \hat{H}), c) = (\text{null}(\hat{H}), c)$ due to rank-nullity theorem. Implying that the maximizing system matrix column comes from the vector space $\text{span}(\mathbf{y})$. \square

The formulation of the problem of the previous Theorem is analogical to the following, which is written using the original system matrix:

$$\min_{\mathbf{z} \in \mathbb{R}^n} \left\{ \rho(\mathbf{y}, L\hat{T}\mathbf{z} \mid C)^2 + \rho(\mathbf{0}, \hat{T}\mathbf{z} \mid \Gamma)^2 \right\}, \quad (40)$$

where

$$\hat{T} = \Gamma^{1/2} \text{Diag} \left(\Gamma^{1/2} L^T (L\Gamma L^T + C)^{-1} L\Gamma^{1/2} \right)^{1/2}. \quad (41)$$

The proper standardized problem involving the back-projection to the original problem uses the transformation

$$T = \Gamma^{1/2} \text{Diag} \left(\Gamma^{1/2} L^T (L\Gamma L^T + C)^{-1} L\Gamma^{1/2} \right)^{1/2} \Gamma^{-1/2}, \quad (42)$$

which yields, in the case of diagonal covariance, the same as the problem 11. Thus, we have presented a natural extension of the technique.

5. Noise robustness of localization via standardized model

Here we consider a case where the assumed Gaussian likelihood model holds, i.e., the measurements are Gaussian distributed. We start by assuming the location of the true source is in the k th node so that $\underline{\mathbf{y}} \sim \mathcal{N}(\hat{\mathbf{L}}_k, C)$. In order for the standardized method to localize the activity correctly, we must have

$$\frac{\left| \hat{\mathbf{L}}_k^T \Sigma^{-1} \underline{\mathbf{y}} \right|}{\sqrt{\hat{\mathbf{L}}_k^T \Sigma^{-1} \hat{\mathbf{L}}_k}} \geq \frac{\left| \hat{\mathbf{L}}_i^T \Sigma^{-1} \underline{\mathbf{y}} \right|}{\sqrt{\hat{\mathbf{L}}_i^T \Sigma^{-1} \hat{\mathbf{L}}_i}} \quad \text{for all } i \in [1, n], \quad (43)$$

where $\Sigma = \hat{L}\hat{L}^T + C$. Without loss of generality, we denote the forward model simply by \hat{L} and assuming the prior model as $\mathcal{N}(\mathbf{0}, I)$ but we could either denote the system matrix by $L\Gamma^{1/2}$ and end up with the same result as the previous section implies. The exact probability that this inequality is true can be derived from the difference of generalized chi-distributed random variables. However, the formulation would be really complex and therefore impractical. So instead, we present a lower bound for the probability that the correct element belongs to the set of reconstruction maxima by its index.

Theorem 5.1. *Assume Gaussian distributed measurements $\underline{\mathbf{y}} \sim \mathcal{N}(\hat{\mathbf{L}}_k, C)$ produced by a point source at k th location. Let*

$$\theta \leq 1 - \text{proj}_{\hat{\mathbf{L}}_k} \left(\hat{\mathbf{L}}_i \mid \Sigma \right), \quad (44)$$

for every $i \in [1, n] \setminus \mathcal{S}(\hat{\mathbf{L}}_k)$. Then the following inequality holds for the probability of the k th standardized parameter attaining the maximum magnitude

$$\mathbb{P} \left(\{k\} \subseteq \arg \max_{i \in [1, n]} \left\{ \frac{\left| \hat{\mathbf{L}}_i^T \Sigma^{-1} \underline{\mathbf{y}} \right|}{\sqrt{\hat{\mathbf{L}}_i^T \Sigma^{-1} \hat{\mathbf{L}}_i}} \right\} \right) \geq \text{Ga} \left(\theta^2 \frac{\lambda_{\min}(\Sigma) \hat{\mathbf{L}}_k^T \Sigma^{-1} \hat{\mathbf{L}}_k}{2\lambda_{\max}(C)}; \frac{m}{2}, 1 \right), \quad (45)$$

where $\lambda_{\max}(\cdot)$ and $\lambda_{\min}(\cdot)$ denotes the largest and smallest eigenvalues of a matrix, respectively.

Proof. The proof aims to estimate the probability of

$$\frac{\left| \hat{\mathbf{L}}_k^T \Sigma^{-1} \underline{\mathbf{y}} \right|}{\sqrt{\hat{\mathbf{L}}_k^T \Sigma^{-1} \hat{\mathbf{L}}_k}} \geq \frac{\left| \hat{\mathbf{L}}_i^T \Sigma^{-1} \underline{\mathbf{y}} \right|}{\sqrt{\hat{\mathbf{L}}_i^T \Sigma^{-1} \hat{\mathbf{L}}_i}} \quad (46)$$

for any $i \in [1, n] \setminus \{k\}$. Let us denote $\mathbf{u} = \Sigma^{-1/2} \hat{\mathbf{L}}_k / \sqrt{\hat{\mathbf{L}}_k^T \Sigma^{-1/2} \hat{\mathbf{L}}_k}$ and $\Sigma^{-1/2} \underline{\mathbf{y}} = \Sigma^{-1/2} \hat{\mathbf{L}}_k + \underline{\mathbf{f}} = \underline{\ell}_k + \underline{\mathbf{f}}$ for simplicity. As we can now see that

$$\frac{\hat{\mathbf{L}}_k^T \Sigma^{-1} \underline{\mathbf{y}}}{\sqrt{\hat{\mathbf{L}}_k^T \Sigma^{-1} \hat{\mathbf{L}}_k}} = \mathbf{u}^T (\underline{\ell}_k + \underline{\mathbf{f}}). \quad (47)$$

The end goal is to estimate an event $Z \geq 0$ for a random number Z defined as

$$Z = \left| \mathbf{u}^T (\underline{\ell}_k + \underline{\mathbf{f}}) \right| - \left| \mathbf{v}^T (\underline{\ell}_k + \underline{\mathbf{f}}) \right|. \quad (48)$$

By decomposing the normalized system matrix column vector \mathbf{v} to $\gamma \mathbf{u} + \sqrt{1 - \gamma^2} \mathbf{u}^\perp$, where $\gamma \in [-1, 1]$, \mathbf{u}^\perp is unit vector and $\mathbf{u}^T \mathbf{u}^\perp = 0$, we can obtain a lower bound for the random variable

$$Z \geq Z^*(\gamma) = \|\underline{\ell}_k\|_2 - |\gamma| \|\underline{\ell}_k\|_2 - \sqrt{1 - \gamma^2} \|\underline{\mathbf{f}}\|_2, \quad (49)$$

and thus $\mathbb{P}(Z^*(\gamma) \geq 0) \leq \mathbb{P}(Z \geq 0)$. Considering $Z^*(\gamma)$ as a function, let us assume that $Z^*(0)$ is positive, i.e., there is more data than noise. Therefore, the expression is positive only when it is bounded by the zero of Z^* :

$$|\gamma| < \frac{\|\underline{\ell}_k\|_2^2 - \|\underline{\mathbf{f}}\|_2^2}{\|\underline{\ell}_k\|_2^2 + \|\underline{\mathbf{f}}\|_2^2} \quad (50)$$

To strict this bound, we obtain

$$\frac{\|\underline{\ell}_k\|_2^2 - \|\underline{\mathbf{f}}\|_2^2}{\|\underline{\ell}_k\|_2^2 + \|\underline{\mathbf{f}}\|_2^2} \geq 1 - \frac{\|\underline{\mathbf{f}}\|_2}{\|\underline{\ell}_k\|_2} \quad (51)$$

Noting that $\gamma = \mathbf{u}^T \mathbf{v}$, we can write an event in the form

$$\|\underline{\mathbf{f}}\|_2 < (1 - |\mathbf{u}^T \mathbf{v}|) \|\underline{\ell}_k\|_2. \quad (52)$$

Because we cannot state anything about the vector \mathbf{v} , we set $\theta \in (0, 1]$ such that $\theta \leq 1 - |\mathbf{u}^T \mathbf{v}|$ for any \mathbf{v} not parallel with \mathbf{u} . Due to the properties of $L2$ -norm

$$\begin{aligned} \|\underline{\mathbf{f}}\|_2 &\leq \|\Sigma^{-1/2} C^{1/2}\| \cdot \left\| \hat{\underline{\mathbf{f}}} \right\|_2 \leq \sqrt{\lambda_{\max}(\Sigma^{-1}) \lambda_{\max}(C)} \left\| \hat{\underline{\mathbf{f}}} \right\|_2 \\ &= \sqrt{\frac{\lambda_{\max}(C)}{\lambda_{\min}(\Sigma)}} \left\| \hat{\underline{\mathbf{f}}} \right\|_2. \end{aligned} \quad (53)$$

As the original random number gets smaller values for each sample than the chi-distributed one, the probability of $\|\underline{\mathbf{f}}\|_2 < (1 - |\mathbf{u}^T \mathbf{v}|) \|\ell_k\|_2$ is larger than with the random number at the end of the previous inequality chain, therefore

$$\begin{aligned} \mathbb{P}(Z \geq 0) &\geq \mathbb{P}(Z^*(\gamma) \geq 0) \\ &\geq \mathbb{P}(\|\underline{\mathbf{f}}\|_2 < \theta \|\ell_k\|_2) \geq \mathbb{P}\left(\sqrt{\frac{\lambda_{\max}(C)}{\lambda_{\min}(\Sigma)}} \|\hat{\underline{\mathbf{f}}}\|_2 < \theta \|\ell_k\|_2\right). \end{aligned} \quad (54)$$

The cumulative distribution of the lower bound at the end of the inequality chain can be expressed via gamma distribution with shape parameter $m/2$ and scale parameter 1. So by opening the expressions

$$\mathbb{P}\left(\sqrt{\frac{\lambda_{\max}(C)}{\lambda_{\min}(\Sigma)}} \|\hat{\underline{\mathbf{f}}}\|_2 < \theta \sqrt{\hat{\mathbf{L}}_k^T \Sigma^{-1} \hat{\mathbf{L}}_k}\right) = \text{Ga}\left(\frac{\theta^2 \hat{\mathbf{L}}_k^T \Sigma^{-1} \hat{\mathbf{L}}_k}{2\lambda_{\max}(C)/\lambda_{\min}(\Sigma)}; \frac{m}{2}, 1\right). \quad (55)$$

□

From the derived inequality, we can see that the lower bound is larger in situations where the noise level is low, and the true source is near the measurement sensors, where the system matrix magnitude is maximized. One could also approximate further by considering a common situation where measurement noise is assumed to be independent and identically distributed with standard deviation σ . Utilizing the inequality $\hat{\mathbf{L}}_k^T \Sigma^{-1} \hat{\mathbf{L}}_k \geq \lambda_{\min}(\Sigma^{-1}) \|\hat{\mathbf{L}}_k\|_2^2 = \lambda_{\max}(\Sigma)^{-1} \|\hat{\mathbf{L}}_k\|_2^2$, one could then write another bound using the signal-to-noise ratio (SNR) defined as the square of the signal mean per variance, i.e., $\|\hat{\mathbf{L}}_k\|_2^2 / \sigma^2$, that reads

$$\mathbb{P}\left(\{k\} \subseteq \arg \max_{i \in [1, n]} \left\{ \frac{|\hat{\mathbf{L}}_i^T \Sigma^{-1} \underline{\mathbf{y}}|}{\sqrt{\hat{\mathbf{L}}_i^T \Sigma^{-1} \hat{\mathbf{L}}_i}} \right\}\right) \geq \text{Ga}\left(\theta^2 \frac{\lambda_{\min}(\Sigma)}{2\lambda_{\max}(\Sigma)} \cdot \text{SNR}; \frac{m}{2}, 1\right). \quad (56)$$

Based on this boundary, there can be at most 2 % of noise (at least 35 dB SNR) in the measurement data to achieve the probability of 0.95 for the conductivity disk used in Figure 1 and independent and identically distributed Gaussian sources. As a drawback of the given boundary, without stating something about the rank of the system matrix and decrease of the modeled signal strength along with distance away from the sensor, the bound is generous for far-field sources.

6. Numerical exmples

This section is divided into three parts. The first part demonstrates that the standardized localization is free from the localization bias of BMNE, and the second one shows the advantage of the introduced generalized formulation (Section 4) in multisource localization and tracking. The third section examines the spatial and noise level-related behavior of the lower bound from Theorem 5.1. In practice, we examine the localization

accuracy statistically reflecting the results to the lower bound. Both parts end with their own results sections.

6.1. Localization of far-field source via BMNE and its standardization

In this example, we give a demonstration of the source localization in a homogenous conductivity disk. Let us assume that we have a far-field source, i.e., far away from the sensors that are on the upper half of the disk in Figure 1. The source is located at point $(0.2, 0.6)$ and the measurements have 5 % of Gaussian white noise. The aim is to localize the source via BMNE without and with standardization.

6.2. results

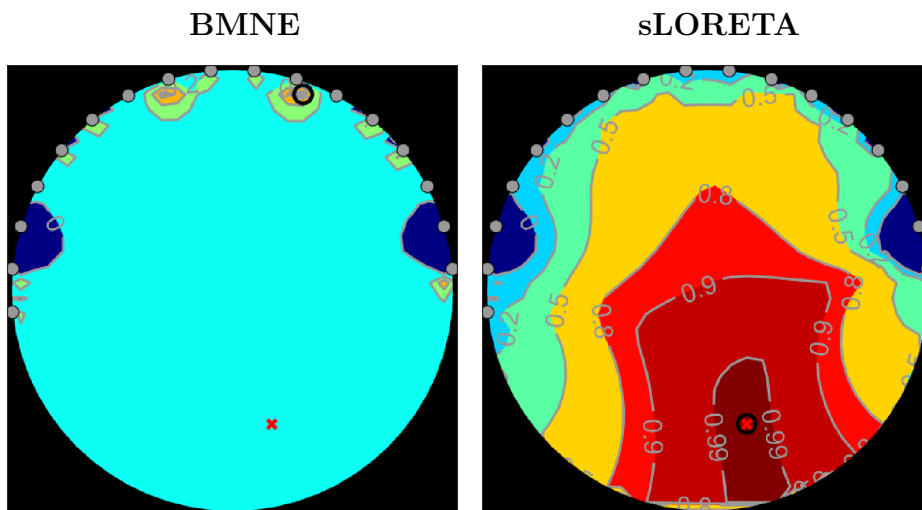


Figure 2. Localization of far-field source located at the position of red cross. The normalized Bayesian minimum norm estimate (BMNE) value map is presented on the left and the normalized value map of standardized BMNE, also called standardized low-resolution brain tomography (sLORETA), is presented on the right. The black ring in both of the pictures shows the location of the maximum reconstruction value where the source is estimated to be.

Figure 2 presents the heat maps of reconstruction values before and after standardization. As we can see, the BMNE value map is biased toward the sensor locations while after standardization (sLORETA) the localization is perfect. The width of the area of high reconstruction values is notably wider for sLORETA than BMNE.

6.3. Unbiasing via standardization and benefits of detailed posterior

6.3.1. Simulation setup In this section, we aim to track and localize a source time series of two sources via the Kalman filter (KF), sLORETA, and Kalman filter for standardized state variables (SKF) [41] whose algorithm is presented in Appendix A. Here we select our evolution model to be a simple random walk for both Kalman filters.

Let the underlying activity inside the previously used homogenous conductivity disk (Figure 1) obey the following evolution model

$$\mathbf{s}_{k+1} = \begin{bmatrix} 0.2 & -0.3 \\ -0.8 & 0.3 \end{bmatrix} \mathbf{s}_k + \begin{bmatrix} f((k+1)\Delta t) \\ 0 \end{bmatrix}, \quad (57)$$

where $f(t) = \exp(-10^5(t - 0.012)^2) \cos(500(t - 0.012) + \pi/2)$. The activity is tracked 25 ms with sampling rate of 1 kHz, yielding $\Delta t = 0.001$. The first source (far-field source) is placed at (0,-0.95), and the second (near-field source) is at (-0.4,0.8). For measurement data creation, we add 5 % of Gaussian noise. One can clearly see that the activities are not independent, which is why the usage of an advanced posterior model could be appropriate. To estimate the Gaussian posterior along the time series, we apply the Kalman filter to demonstrate the advantage of a detailed posterior model. In the Bayesian sense, the Kalman filter gives a Gaussian posterior for each time step with updated mean and covariance, therefore, based on the section 4, we are able to apply standardization technique to it as a post-hoc weighting, where the weights are updated at every time step.

In the discretization of the analytical forward model, we apply a regular grid of 650 nodes in the disk. For inversion, we form another grid with 30 % fewer points to avoid an inverse crime. To track the activity, we listen to the location of true sources and track the reconstruction value evolution in those regions.

In localization, we utilize the opposite polarity of the time evolutions. This way, we estimate the location of both sources at every time step by seeking the minimum and maximum value of the reconstruction. Finally, we will assign a Gaussian mixture model to find two clusters that aid in interpreting the localization results.

6.3.2. Results Considering the localization results in Figure 3, the Kalman filter is able to localize the near-field source with fair accuracy even if the variability in individual localization at different time steps is large. As KF is analogical to BMNE, the localization bias is prominent since the estimations are accumulated on the upper boundary. sLORETA is able to localize the near-field source with higher accuracy and with less variety than KF. Surprisingly, sLORETA cannot localize the far-field source even if it is detecting signals inside the disk, and therefore, it does not exhibit bias of BMNE. SKF, as a combination of both techniques, is capable of localizing both sources. Variety in near-field localization estimates is slightly lower than with sLORETA as the 75 % confidence ellipse is a bit smaller. No individual near-field estimation hit the target perfectly but the cluster mean is within sub-mesh accuracy from the true location of the source.

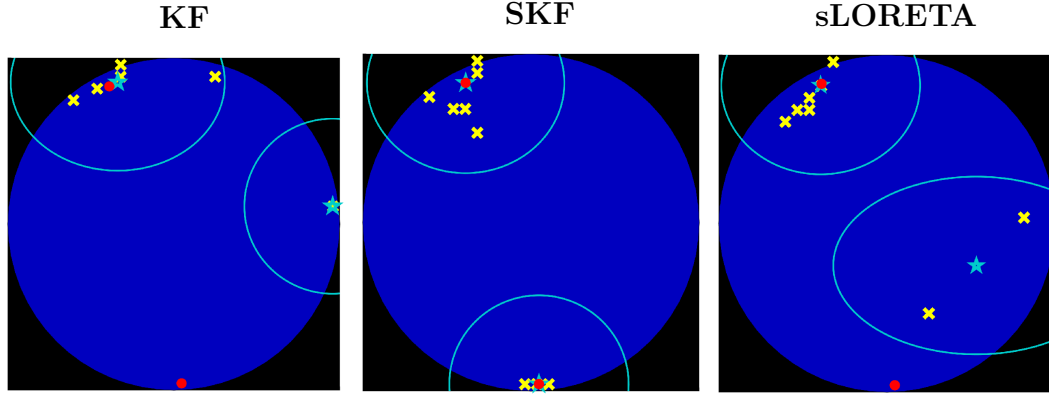


Figure 3. Localization estimates at each time point starting from 6 ms, when the far-field source starts effect. Individual estimates are indicated by yellow crosses, red balls show the location of true sources, and a 75 % confidence ellipse of the 2-component Gaussian mixture model is presented in turquoise. The used methods from left to right are the Kalman filter (KF), standardized Kalman filter (SKF), and standardized low-resolution brain tomography (sLORETA).

From the tracking results in Figure 4, we obtain that Kalman filter is tracking the source near sensors, but the relative strength of the far source is suppressed. sLORETA follows the near-field source well, but the far-field source's track follows the other one and seems to not have independent tracks as one could desire. Contrarily, Kalman filter for standardized states can track both of the activities independently at the beginning of the oscillation. The latter part of the far-field track is almost identical to the sLORETA's track.

6.4. Localization accuracy from noisy measurements

6.4.1. Simulation setup The purpose of these experiments is to demonstrate the spatial (I) and SNR (II) dependence of the lower bound from theorem 5.1 and its relation to actual localization accuracy via reconstruction. We have a great interest in how close the bound is to the localization accuracy statistics observed in simulations.

In example (I), we place a true source in each mesh node once and then calculate 10,000 samples of measurement with Gaussian noise using 5 % and 15 % of noise. After that, we use the standardized reconstruction technique to recover the location of the true source while keeping track of how often the maximum absolute value of reconstructions hits the target. From this, we can draw a contour map over the unit disk and compare it with the map of the lower bound.

In example (II), we take three points from the y-axis and calculate the reconstructions and localization success percentage similarly to experiment (I). This time, we use multiple noise levels. The true sources are located from (0,0.90) to (0,0.6) in decrements of 0.1.

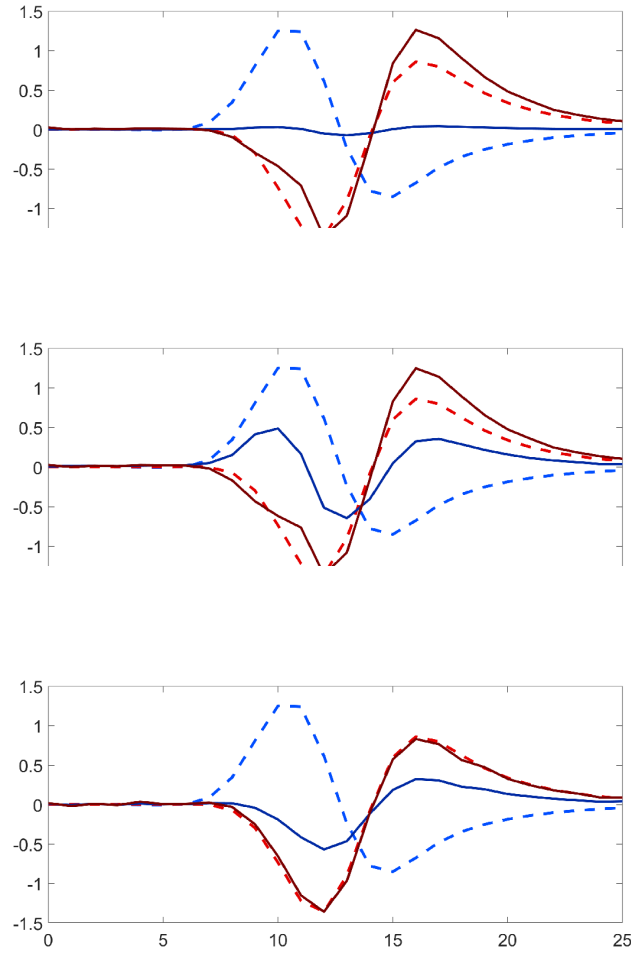


Figure 4. Track of the source activity at the correct location running along with the time that is expressed in milliseconds. Dashed lines represent the true track and solid lines represent the estimated tracks. Blue lines are for the far-field source and red lines are for the near-field source. The used methods from top to bottom are the Kalman filter (KF), standardized Kalman filter (SKF), and standardized low-resolution brain tomography (sLORETA).

6.4.2. Results By looking at the spatial probability maps of actual reconstruction to localize correctly and the lower bound of that in Figure 5, we can see the gap between sampled reality and the bound being closest to each other near sensors. The lower bound drops quickly along the distance from measurement sensors, much quicker than in the sampled case. In the 5 % noise case, the standardized reconstruction is accurate almost everywhere with a probability higher than 0.9 except at the region most far away from the sensors. At 15 % the region of over 0.9 probability has shrunk by about half and patterns of lower probability pools emerge near sensors. The lower bound has only a small over 0.9 probability area on the left side of the models near the second sensor in clockwise order. The SNR tendency of the sampled probability and the lower bound at different depths in Figure 6 shows small gaps between probability curves at high SNR (low percent) but the curves diverge faster the deeper the situation is examined. If

we say the curves are divergent when the difference is higher than 0.01, the divergence points are at 13, 9, 6, and 3.5 % for points from 0.9 to 0.6 in decrements of 0.1.

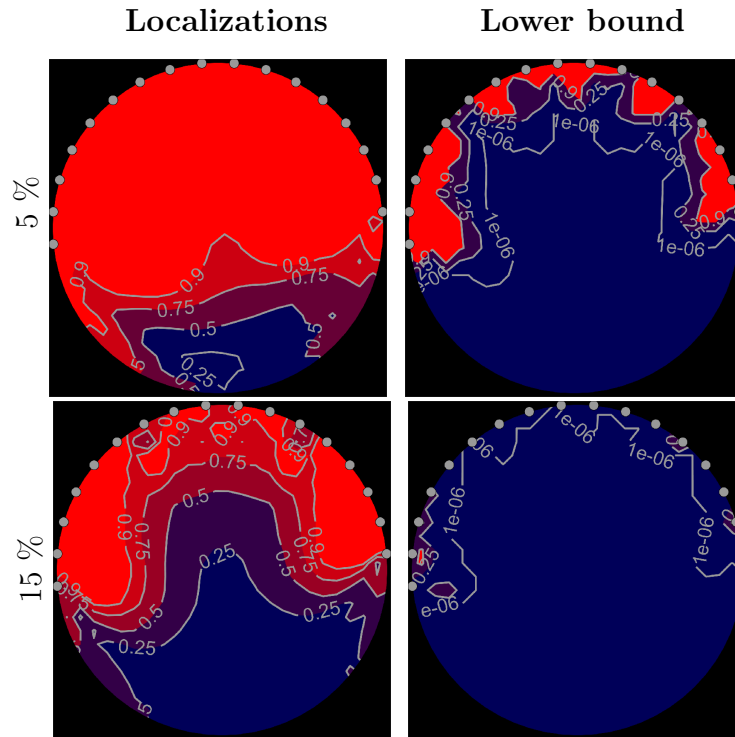


Figure 5. Sampled probability of the standardized inversion to find the correct source location (**left**) mapped over the unit disk and the spatial contours of the lower bound from Theorem 5.1 (**right**). The upper row presents the results when 5 % of the noise is applied to the measurements and the lower row shows the same results for 15 % of noise.

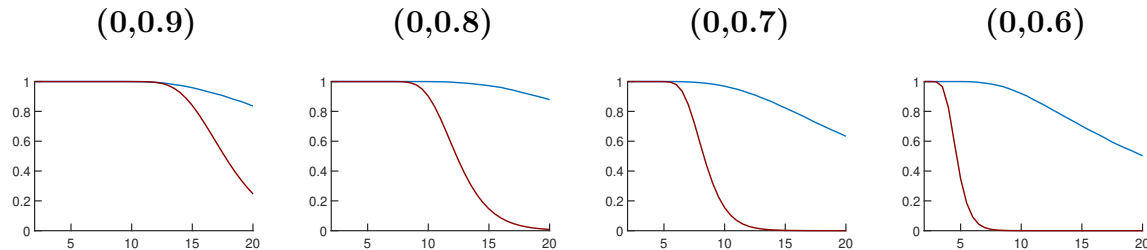


Figure 6. Sampled probability of the standardized inversion to find the correct source location (**blue**) from noise levels from 2 % to 20 %. The red curve shows the behavior of the lower bound. Different graphs are calculated at different points of the y-axis and the locations are presented above the graphs

7. Discussion and conclusions

This paper considers the standardization technique that is well-merited in the electromagnetic inverse source problem [34, 35, 36, 42] described here for the general

linearized Poisson problem with Neumann boundary condition. The bias of minimum norm estimation due to the maximum principle is demonstrated as well as how standardization can reduce this bias in the statistical sense utilizing the orthogonal decomposition of the system matrix. Then, the inverse technique is generalized for any Bayesian model of Gaussian posterior, i.e., Gaussian process regression problem, and its analogy to the original presentation (sLORETA) that assumes independently and identically distributed Gaussian recovering variables. We also derived a lower bound for the probability that the method localizes the source perfectly under Gaussian distributed measurements. The results show that even if the correct source location is found with a forward model that fully describes reality, the set of solutions may be larger than one point if the simulated measurements produced from different sources are not distinct enough. This could, for example, be realized in a situation where the source configuration can have sources near and far with respect to the measurement sensors, the only difference of which is the strength of the measurement signal. Because the technique standardizes the possible solutions in relation to the location, the strength of the signal no longer has an effect. Therefore, one must design the Gaussian prior model with care to pick the most probable source location from the feasible set provided via standardization. Even if it is demonstrated previously that the standardized method utilizing Gaussian posterior cannot recover multiple simultaneous sources when independent and identically distributed sources are assumed as *a priori* [37, 38], our results suggest that this is not the case with more complex Gaussian priors, particularly the one provided via Kalman filter, that are viable via introduced Bayesian generalization of the technique itself. Moreover, using the Bayesian extension of standardization, the technique could be coupled with any conditionally Gaussian model having hyperpriors, for example, gamma, inverse gamma [2], or half-Cauchy distribution [43] as the hyperprior model.

The probability limit for perfect localization explains why high noise robustness is obtained when the true source is located near measurement sensors [32, 33]. Even though the presented lower limit compares weakly to the hit rate of practical localization for far-field sources and with particularly high noise levels, the limit could have its uses in the estimation of high p-values for common low noise and near-field cases, where sources of error could be said to be mostly modeling-originated. In actual measurement procedures, the noise level is not necessarily very high due to the averaging over multiple trials, and because of possible unfavorable sensor positioning and forward model parameters or uncertainty of those, the purely inverse modeling-based accuracy of localization is overshadowed by the practical sources of errors.

Acknowledgment

The author would like to thank his supervisors Prof. Sampsa Pursiainen and Dr. Alexandra Koulouri for discussions on this work. The author is supported by the Jenny and Antti Wihuri Foundation.

Appendix A. Standardized Kalman Filter

Let us use a typical linear dynamical model

$$\mathbf{y}_t = L\mathbf{x}_t + \mathbf{r}_t, \quad (\text{A.1})$$

$$\mathbf{x}_t = A_t\mathbf{x}_{t-1} + \mathbf{q}_t, \quad (\text{A.2})$$

where $\mathbf{r}_t \sim \mathcal{N}(\mathbf{0}, R_t)$ and $\mathbf{q}_t \sim \mathcal{N}(\mathbf{0}, Q_t)$. Then, the prediction step is calculated as the following

$$\begin{aligned} \mathbf{x}_{t|t-1} &= A_t\mathbf{x}_{t-1|t-1} \\ P_{t|t-1} &= A_tP_{t-1|t-1}A_t^T + Q_t \end{aligned}$$

and the update step is

$$\begin{aligned} S_t &= LP_{t|t-1}L^T + R_t \\ K_t &= P_{t|t-1}L^TS_t^{-1} \\ \mathbf{x}_{t|t} &= \mathbf{x}_{t|t-1} + K_t(\mathbf{y}_t - L\mathbf{x}_{t|t-1}) \\ P_{t|t} &= P_{t|t-1} - K_tS_tK_t^T \\ W_t &= P_{t|t-1}^{1/2}\text{Diag}\left(P_{t|t-1}^{-1/2}K_tS_tK_t^TP_{t|t-1}^{-1/2}\right)^{-1/2}P_{t|t-1}^{-1/2} \\ \mathbf{z}_{t|t} &= W_t\mathbf{x}_{t|t}. \end{aligned}$$

The second last step introduces the time-depend post-hoc weights consisting of inversion of matrix square root of the prior covariance matrix and the diagonal matrix, where $\text{Diag}(\cdot)$ forms a diagonal matrix with the same diagonal elements as in the input matrix. The formulation of the weighting matrix is derived from the equation (42). Vector $\mathbf{z}_{t|t}$ gives the standardized Kalman estimation at time step t .

References

- [1] Roberta Grech, Tracey Cassar, Joseph Muscat, Kenneth P Camilleri, Simon G Fabri, Michalis Zervakis, Petros Xanthopoulos, Vangelis Sakkalis, and Bart Vanrumste. Review on solving the inverse problem in EEG source analysis. *Journal of neuroengineering and rehabilitation*, 5(1):25–25, 2008.
- [2] Daniela Calvetti, Harri Hakula, Sampsa Pursiainen, and Erkki Somersalo. Conditionally Gaussian Hypermodels for Cerebral Source Localization. *SIAM Journal on Imaging Sciences*, 2(3):879–909, 2009.
- [3] Guofa Shou, Ling Xia, and Mingfeng Jiang. Solving the Electrocardiography Inverse Problem by Using an Optimal Algorithm Based on the Total Least Squares Theory. In *Third International Conference on Natural Computation (ICNC 2007)*, volume 5, pages 115–119. IEEE, 2007.
- [4] G. E. Backus and J. F. Gilbert. Numerical applications of a formalism for geophysical inverse problems. *Geophysical Journal of the Royal Astronomical Society*, 13(1-3):247–276, 1967.
- [5] T.C Johnson and D Wellman. Accurate modelling and inversion of electrical resistivity data in the presence of metallic infrastructure with known location and dimension. *Geophysical journal international*, 202(2):1096–1108, 2015.
- [6] Wenyang Shi, Guangzhi Yin, Mi Wang, Lei Tao, Mengjun Wu, Zhihao Yang, Jiajia Bai, Zhengxiao Xu, and Qingjie Zhu. Progress of electrical resistance tomography application in oil and gas reservoirs for development dynamic monitoring. *Processes*, 11(10):2950–, 2023.

- [7] Thomas R Knösche and Jens Haueisen. *EEG/MEG Source Reconstruction: Textbook for Electro-And Magnetoencephalography*. Springer International Publishing AG, Cham, 2022.
- [8] Bart Vanrumste, Gert Van Hoey, Rik Van de Walle, Michel R.P. D’Havé, Ignace A. Lemahieu, and Paul A.J.M. Boon. Comparison of performance of spherical and realistic head models in dipole localization from noisy EEG. *Medical engineering & physics*, 24(6):403–418, 2002.
- [9] Federica Vatta, Fabio Meneghini, Fabrizio Esposito, Stefano Mininel, and Francesco Di Salle. Realistic and Spherical Head Modeling for EEG Forward Problem Solution: A Comparative Cortex-Based Analysis. *Computational Intelligence and Neuroscience*, 2010:972060–11, 2010.
- [10] Dafang Wang, Robert M. Kirby, and Chris R. Johnson. Finite-Element-Based Discretization and Regularization Strategies for 3D Inverse Electrocardiography. *IEEE transactions on biomedical engineering*, 58(6):1827–1838, 2011.
- [11] Bradley Efron, Trevor Hastie, Iain Johnstone, and Robert Tibshirani. Least angle regression. *The Annals of statistics*, 32(2):407–451, 2004.
- [12] Manfred Fuchs, Michael Wagner, Thomas Köhler, and Hans-Aloys Wischmann. Linear and Nonlinear Current Density Reconstructions. *Journal of clinical neurophysiology*, 16(3):267–295, 1999.
- [13] Kensuke Sekihara and Srikatan S. Nagarajan. *Adaptive Spatial Filters for Electromagnetic Brain Imaging*. Series in Biomedical Engineering. Springer Berlin Heidelberg, Berlin, Heidelberg, 1st ed. 2008. edition, 2008.
- [14] R D Pascual-Marqui. Standardized low-resolution brain electromagnetic tomography (sLORETA): technical details. *Methods and findings in experimental and clinical pharmacology*, 24:5–12, 2002.
- [15] Frank Neugebauer, Marios Antonakakis, Kanjana Unnwongse, Yaroslav Parpaley, Jörg Wellmer, Stefan Rampp, and Carsten H Wolters. Validating EEG, MEG and combined MEG and EEG beamforming for an estimation of the epileptogenic zone in focal cortical dysplasia. *Brain sciences*, 12(1):114–, 2022.
- [16] Joonas Lahtinen, Fernando Moura, Maryam Samavaki, Samuli Siltanen, and Sampsa Pursiainen. In silico study of the effects of cerebral circulation on source localization using a dynamical anatomical atlas of the human head. *Journal of neural engineering*, 20(2):26005–, 2023.
- [17] Jari. Kaipio and E. Somersalo. *Statistical and Computational Inverse Problems*. Applied Mathematical Sciences, 160. Springer New York, New York, NY, 1st ed. 2005. edition, 2005.
- [18] M.S Hämäläinen and R.J Ilmoniemi. Interpreting magnetic fields on the brain: minimum norm estimates. *Medical & biological engineering & computing*, 32(1):35–42, 1994.
- [19] Murray H. Protter and Hans F. Weinberger. *Maximum principles in differential equations*. Englewood Cliffs (N.J.), 1967.
- [20] Jürgen. Jost. *Partial Differential Equations*. Graduate Texts in Mathematics, 214. Springer New York, New York, NY, 2nd ed. 2007. edition, 2007.
- [21] T. A. Crowley, C. D. Haupt, and D. B. Kynor. A Weighting Matrix to Remove Depth Bias in the Linear Biomagnetic Inverse Problem with Application to Cardiology. In Cheryl J. Aine, Gerhard Stroink, Charles C. Wood, Yoshio Okada, and Stephen J. Swithenby, editors, *Biomag 96*, pages 197–200, New York, NY, 2000. Springer New York.
- [22] Yohan Attal and Denis Schwartz. Assessment of subcortical source localization using deep brain activity imaging model with minimum norm operators: a MEG study. *PloS one*, 8(3):e59856–e59856, 2013.
- [23] Roberto D. Pascual-Marqui, Dietrich Lehmann, Martha Koukkou, Kieko Kochi, Peter Anderer, Bernd Saletu, Hideaki Tanaka, Koichi Hirata, E. Roy John, Leslie Prichep, Rolando Biscay-Lirio, and Toshihiko Kinoshita. Assessing interactions in the brain with exact low-resolution electromagnetic tomography. *Philosophical transactions of the Royal Society of London. Series A: Mathematical, physical, and engineering sciences*, 369(1952):3768–3784, 2011.
- [24] Ole Løseth Elvetun and Bjørn Fredrik Nielsen. Weighted sparsity regularization for source identification for elliptic PDEs. *Journal of inverse and ill-posed problems*, 31(5):687–709, 2023.
- [25] Meijian An. A simple method for determining the spatial resolution of a general inverse problem.

- Geophysical journal international*, 191(2):849–864, 2012.
- [26] George Backus and Freeman Gilbert. The Resolving Power of Gross Earth Data. *Geophysical Journal of the Royal Astronomical Society*, 16(2):169–205, 1968.
 - [27] Rolando Grave de Peralta Menendez, Olaf Hauk, Sara Gonzalez Andino, Hermann Vogt, and Christoph Michel. Linear inverse solutions with optimal resolution kernels applied to electromagnetic tomography. *Human brain mapping*, 5(6):454–467, 1997.
 - [28] Xiaohong Wan, Atsushi Sekiguchi, Satoru Yokoyama, Jorge Riera, and Ryuta Kawashima. Electromagnetic source imaging: Backus-Gilbert resolution spread function-constrained and functional MRI-guided spatial filtering. *Human brain mapping*, 29(6):627–643, 2008.
 - [29] Meijian An. On Resolution Matrices. *Pure and applied geophysics*, 180(1):111–143, 2023.
 - [30] Roberto D Pascual-Marqui. Discrete, 3D distributed, linear imaging methods of electric neuronal activity. Part 1: exact, zero error localization. *arXiv.org*, 2007.
 - [31] Kensuke Sekihara, Maneesh Sahani, and Srikantan S Nagarajan. Localization bias and spatial resolution of adaptive and non-adaptive spatial filters for MEG source reconstruction. *NeuroImage (Orlando, Fla.)*, 25(4):1056–1067, 2005.
 - [32] Matthias Dümpelmann, Tonio Ball, and Andreas Schulze-Bonhage. sLORETA allows reliable distributed source reconstruction based on subdural strip and grid recordings. *Human brain mapping*, 33(5):1172–1188, 2012.
 - [33] Sajib Saha, Ya I Nesterets, M Tahtali, and T E Gureyev. Evaluation of spatial resolution and noise sensitivity of sLORETA method for EEG source localization using low-density headsets. *Biomedical physics & engineering express*, 1(4):45206–, 2015.
 - [34] Karin L. de Gooijer-van de Groep, Frans S.S. Leijten, Cyrille H. Ferrier, and Geertjan J.M. Huiskamp. Inverse modeling in magnetic source imaging: Comparison of MUSIC, SAM(g2), and sLORETA to interictal intracranial EEG. *Human brain mapping*, 34(9):2032–2044, 2013.
 - [35] Ana Coito, Silke Biethahn, Janina Tepperberg, Margherita Carboni, Ulrich Roelcke, Margitta Seeck, Pieter Mierlo, Markus Gschwind, and Serge Vulliemoz. Interictal epileptogenic zone localization in patients with focal epilepsy using electric source imaging and directed functional connectivity from low-density EEG. *Epilepsia open*, 4(2):281–292, 2019.
 - [36] Rui Li, Chris Plummer, Simon J. Vogrin, William P. Woods, Levin Kuhlmann, Ray Boston, David T.J. Liley, Mark J. Cook, and David B. Grayden. Interictal spike localization for epilepsy surgery using magnetoencephalography beamforming. *Clinical neurophysiology*, 132(4):928–937, 2021.
 - [37] Michael Wagner, Manfred Fuchs, and Jörn Kastner. Evaluation of sLORETA in the presence of noise and multiple sources. *Brain topography*, 16(4):277–280, 2004.
 - [38] Mohd Faizal Mohd Zulkifly, Albert Lehr, Daniel van de Velden, Asad Khan, Niels K Focke, Carsten H Wolters, and Walter Paulus. Directionality of the injected current targeting the P20/N20 source determines the efficacy of 140 Hz transcranial alternating current stimulation (tACS)-induced aftereffects in the somatosensory cortex. *PloS one*, 17(3):e0266107–e0266107, 2022.
 - [39] Alberto J.R Leal, Ana I Dias, José P Vieira, Ana Moreira, Luís Távora, and Eulália Calado. Analysis of the dynamics and origin of epileptic activity in patients with tuberous sclerosis evaluated for surgery of epilepsy. *Clinical neurophysiology*, 119(4):853–861, 2008.
 - [40] A Björck. A Schur method for the square root of a matrix. *Linear algebra and its applications*, 52-53(1):127–140, 1983.
 - [41] Joonas Lahtinen, Paavo Ronni, Narayan Puthanmadam Subramaniyam, Alexandra Koulouri, Carsten Wolters, and Sampsa Pursiainen. Standardized kalman filtering for time serial source localization of simultaneous subcortical and cortical brain activity. www.techrxiv.org/722443/UqPLPdTHCJ-oxYE2bCoI6Q, 2024.
 - [42] Daniel van de Velden, Ev-Christin Heide, Caroline Bouter, Jan Bucerius, Christian H. Riedel, and Niels K. Focke. Effects of inverse methods and spike phases on interictal high-density EEG source reconstruction. *Clinical neurophysiology*, 156:4–13, 2023.

- [43] Yiqiu Dong and Monica Pragliola. Inducing sparsity via the horseshoe prior in imaging problems. *Inverse problems*, 39(7):74001–, 2023.